ISSN 0015-4628, Fluid Dynamics, 2016, Vol. 51, No. 3, pp. 381–388. © Pleiades Publishing, Ltd., 2016.
Original Russian Text © A.S. Lobasov, A.V. Minakov, V.Ya. Rudyak, 2016, published in Izvestiya Rossiiskoi Akademii Nauk, Mekhanika Zhidkosti i Gaza, 2016, Vol. 51, No. 3, pp. 89–98.

Viscosity Effect on the Flow Patterns in T-Type Micromixers

A. S. Lobasov[a,b,c], A. V. Minakov[a,b,c], and V. Ya. Rudyak[c]

[a] *Kutateladze Institute of Thermophysics, Siberian Branch, Russian Academy of Science, pr. Akademika Lavrent'eva 1, Novosibirsk, 630090 Russia*

[b] *Siberian Federal University, pr. Svobodnyi 79, Krasnoyarsk, 660041 Russia*

[c] *The Novosibirsk State University of Architecture and Civil Engineering, ul. Leningradskaya 113, Novosibirsk, 630008 Russia*

e-mail: perpetuityrs@mail.ru

Received May 20, 2015

Abstract—Flow patterns and mixing of liquids with different viscosities in T-type micromixers are numerically investigated on the Reynolds number range from 1 to 250. The viscosity ratio of the mixing media varied from 1 to 2; its effect on the flow structure and the mixing is studied. The dependences of the mixing efficiency and the pressure difference in the channel on the viscosity ratio and the Reynolds number are obtained. It is shown that the viscosity ratio has a considerable effect on the flow structure before and after transition from the symmetric to the asymmetric flow pattern. The self-similar behavior of the asymmetric flow pattern is established.

Keywords: fluid dynamics, numerical modeling, T-shaped microchannel, micromixer, mixing, viscosity, SigmaFlow CFD package.

DOI: 10.1134/S0015462816030108

In recent years, the miniaturization of engineering devices has become topical, while micromechanics has become an intensely developing and promising field of research. Microchannel devices are widely used in different fields of science and engineering as micro heat exchangers, micromixers, and microfilters. The operation of most of microchannel devices employed in chemistry and biology requires rapid and effective mixing of materials [1–5]. However, flows in microchannels are primarily laminar and the mixing proceeds by diffusion and, therefore, vary slowly. For this reason, the development and optimization of micromixers with a minimum mixing time is the topical problem in the development of microchannel devices.

Usually, it is laminar, low-Reynolds-number flows, typical in microfluidics, that are considered in most of micromixers. However, in practice situations can occur, where the Reynolds numbers in microflows are fairly high. Moreover, at relatively high Reynolds numbers some new interesting phenomena can be observable in the microchannels; these need to be investigated both from the fundamental standpoint and for practical purposes.

The first investigation of the mixing of liquids in a T-shaped microchannel at moderate Reynolds numbers was apparently presented in [6]. In that study it was for the first time experimentally shown that for certain values of the flow velocity at the T-type micromixer entry the mixing can be particularly effective.

The mixing in a T-shaped channel at low Reynolds numbers was numerically modeled in [7]. The effect of the transverse dimensions of the channel and the angle between the entry regions of the mixer and the mixing channel on the mixing path was investigated.

The most complete experimental investigation in a T-shaped microchannel at moderate Reynolds numbers (100 to 400) was carried out in [8]. Using micro laser induced fluorescence (μ-LIF) and micro particle image velocimetry (μ-PIV) the velocity and concentration fields were determined in different mixer sections and the mixing efficiency was measured for the first time.

The set of numerical and experimental studies [9–12] should also be noted. In those studies certain flow regimes in T-shaped microchannels with different cross-sections were calculated. The existence of a critical Reynolds number at which the Dean vortices in a T-shaped microchannel lose the symmetry was experimentally shown. It was established that for the $600 \times 300 \times 300$ μm channel the critical Reynolds number is about 150. This value was shown to strongly depend on the channel dimensions.

This effect was considered in more detail in the cycle of studies [13–15]. The flow and mixing regimes for the water-water system in a T-type micromixer were investigated on the wide Reynolds number range from 1 to 1000 using the numerical modeling and the μ-PIV and μ-LIF measurements. The flow structure and its effect on the mixing were investigated. Altogether, five different flow patterns were found to exist. The dependences of the friction coefficient and the mixing efficiency on the Reynolds number were obtained. A sharp increase in the mixing efficiency on transition from the steady symmetric to the steady asymmetric flow pattern was discovered. The laminar-turbulent transition region was investigated. Good qualitative and quantitative agreement with the experimental results was obtained.

The purpose of this study is to systematically investigate the effect of the viscosity ratio of mixing liquids on the flow and mixing regimes in T-type micromixers. The topicality of this study is due to the practical interest, since in practice it is usually liquids with different viscosities that are subjected to mixing.

1. MATHEMATICAL MODEL AND NUMERICAL ALGORITHM

In this study, we will consider incompressible flows of multicomponent Newtonian fluids described using the hydrodynamic approach based on the solution of the Navier–Stokes equations. At present, in many experiments it is established that for liquids this description performs well up to the channel dimensions of the order of 1 μm.

The general form of the Navier–Stokes equations is as follows:

$$\begin{aligned} &\partial\rho/\partial t + \nabla(\rho\mathbf{v}) = 0, \\ &\partial\rho\mathbf{v}/\partial t + \nabla(\rho\mathbf{v}\mathbf{v}) = -\nabla p + \nabla\mathbf{T}. \end{aligned} \tag{1.1}$$

Here, ρ is the fluid density, p is the pressure, $\mathbf{v}$ is the velocity, and $\mathbf{T}$ is the viscous stress tensor, whose components are determined as follows:

$$\mathbf{T}_{ij} = \mu\left(\frac{\partial U_j}{\partial x_i} + \frac{\partial U_i}{\partial x_j}\right),$$

where μ is the mixture viscosity and u_i are the velocity vector components.

The mixture viscosity is determined in terms of the mass fractions of its components f_i and the molecular viscosities μ_i of the pure components

$$\mu = \sum_i f_i\mu_i.$$

The mixture density is determined in terms of the mass concentrations f_i of the flow components and the partial densities ρ_i as follows:

$$\rho = \left[\sum_i (f_i/\rho_i)\right]^{-1}.$$

The evolution of the mass concentrations is governed by the equation

$$\partial\rho f_i/\partial t + \nabla(\rho f_i\mathbf{v}) = \nabla(\rho D_i\nabla f_i). \tag{1.2}$$

where D_i is the diffusion coefficient of component i.

The no-slip conditions are imposed on the channel walls. The applicability of these conditions for the channels with the dimensions of about 50 μm was shown in [1, 14–16].

The above system of equations was solved using the σFlow software package for the computational fluid dynamics problems. The detailed description of the numerical algorithm used in this program is given

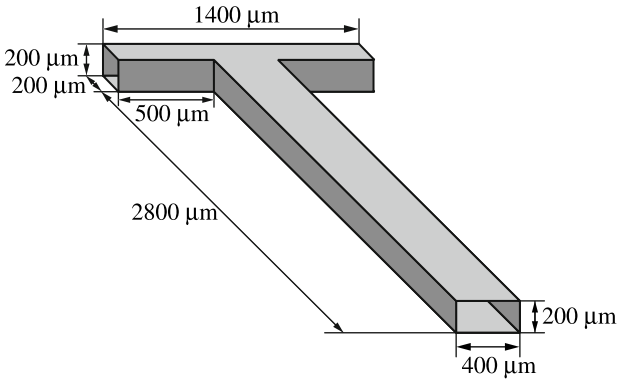

Fig. 1. Geometry of the problem.

in [17]. Here, we note the main aspects of the numerical technique. The difference counterpart of the convection-diffusion equations (1.1), (1.2) is determined using the finite volume method [18–20] for structured multi-block grids. The difference scheme thus obtained is automatically conservative. The essence of the method is in subdividing the computation domain into control volumes and integrating the original conservation equations over any control volume for the purpose of obtaining finite-difference relations. The convective terms of the transport equations (1.1) and (1.2) are approximated using the upwind second-order schemes QUICK [21] and TVD [22], respectively. The time-dependent terms of the fluid dynamics equations are approximated using an implicit second-order scheme. The diffusion fluxes and the source terms are approximated by the finite-volume counterparts of central difference relations with the second order of accuracy. The relation between the velocity and pressure fields ensuring the fulfillment of the continuity equation is realized using the SIMPLEC procedure on conjugate grids. The Rhie–Chou approach is applied to eliminate the pressure field oscillations; it consists in introducing a monotonizator into the equations for the pressure correction [22]. The difference equations obtained as a result of the discretization of the original system of differential equations are solved by means of an iteration procedure using an algebraic multigrid solver [23].

In the calculations a four-block grid consisting of 4.5 millions gridpoints was used. A constant flow rate with a developed velocity profile was preassigned at the entry. The von Neumann conditions were preassigned at the mixing channel entry; they mean the equality to zero of the derivatives of all scalar quantities with respect to the normal to the exit. The channel dimensions are presented in Fig. 1. The channel thickness is about 200 μm and the widths of its narrow and wide sections are about 200 and 400 μm.

In the calculations the pressure difference between one of the mixer entries and its exit was calculated, together with the mixing efficiency. In the scientific literature the efficiency is evaluated using the parameter $M = 1 - \sigma/\sigma_0$, where $\sigma = V^{-1}\int_V (f - \langle f\rangle)^2\, dV$ is the r.m.s. deviation of the concentration of component f from its mean value $\langle f\rangle$ and $\sigma_0 = \langle f\rangle(1 - \langle f\rangle)$ is the maximum r.m.s. deviation. Sometimes a parameter characterizing the mixture dispersity, $\Phi = V^{-1}\int_V |\nabla f|\, dV$, is also used; this is the mean value of the mixture component concentration gradient. This quantity is also called the diffusion potential.

2. RESULTS OF THE NUMERICAL MODELING

Mixing of two liquids with the same properties. We will first consider the case of the mixing of two liquids with the same properties. Pure water is supplied to the mixer through one of its entries at the flow rate Q. Water colored with rhodamine is supplied through the other entry at the same flow rate. The densities of both liquids are 1000 kg/m^3, viscosities are 0.001 Pa s, and the dye diffusivity in the water $D = 2.63 \times 10^{-10}$ m^2/s. As noted above, a detailed investigation of the flow patterns and the mixing of water and water colored by rhodamine was made in [13–15]. Here, these flow patterns will be described only briefly. The change of the

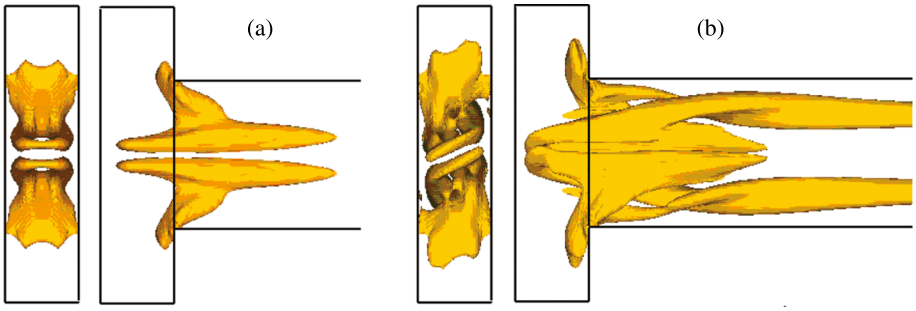

Fig. 2. λ_2 isosurfaces; Re = 140 (a) and 150 (b); the left sides of the figures represent the view from the dead wall of the mixer and the right sides are the side views.

flow patterns in the microchannel is characterized by the Reynolds number determined as follows:

$$\mathrm{Re} = (\rho U d_h)/\mu,$$

where $U = Q/(2\rho H^2)$ is the mean-flow-rate velocity in the mixing channel, $H = 200$ μm is the channel height, and $d_h = 267$ μm is the hydraulic diameter.

For the Reynolds numbers of the order of unity a creeping rotationless flow is observable; the dye mixing is fairly weak. With increase in the Reynolds number a pair of symmetric horseshoe-shaped vortices are formed in the mixer near its left dead-end wall and propagate into the mixing channel (Fig. 2a). In the mixing channel these vortices gradually decay. The horseshoe-shaped vortices arise due to the development of secondary flows induced by the centrifugal force arising as a result of the flow turn. They are called the Dean vortices. The horseshoe-shaped structure of the Dean vortices is shown in Fig. 2a in the form of the λ_2 isosurface. As can be seen in the figure, in this case the flow is symmetric about the central longitudinal plane of the mixer. Any vortical horseshoe is within the limits of one liquid and does not intersect the interface of the mixing media. For this reason, the interface remains almost plane.

As the Reynolds number is further increased, a very interesting flow restructuring can be observable. Starting from the Reynolds number of about 145, owing to the Kelvin–Helmholtz instability development, the pair of the horseshoe-shaped vortices turns by an angle of 30° to the central longitudinal plane of the mixer (Fig. 2b). Due to this flow turnover, one branch of the horseshoe-shaped vortex gradually decays, whereas the intensity of the other branch increases. Ultimately, two intense, identically swirled vortices are formed in the mixing channel (Fig. 2b). However, the flow remains steady! Since in the nonsymmetric regime the vortex intensity considerably increases, they extend through the mixing channel up to its exit. The presence of flow swirling in the mixing channel leads to the formation of a layered S-shaped structure consisting of mixing liquids (Fig. 3b). In this structure the surface of the contact between the two mixing liquids is fairly developed which leads to a sharp increase in the mixing efficiency. On transition from the symmetric flow pattern (Re $<$ 145) to the nonsymmetric regime (Re $>$ 145) the mixing efficiency increases by a factor of more than 25.

The Reynolds-number-dependence of the mixing efficiency is presented in Fig. 4a (curve *1*). As distinct from the earlier studies [13–15], in this study the mixing efficiency is calculated with a very small step with respect to the Reynolds number. Thus, it is for the first time shown that symmetric-to-nonsymmetric flow pattern transition occurs almost jumpwise. Thus, in particular, the symmetric flow regime is observable at Re = 144, while already at Re = 144.5 the flow turns up. It is interesting to note that this important flow restructuring has almost no effect on the pressure difference between the mixer entry and exit (Fig. 4b, curve *1*).

Without any considerable variations, the vortex structure of the steady flow described above continues to exist on the Reynolds number range from 145 to about 240. At higher Reynolds numbers the flow is no longer steady. On the 240 $<$ Re $<$ 400 range it can be regarded as periodic. At the Reynolds numbers greater than 600 the flow in this channel becomes turbulent [14].

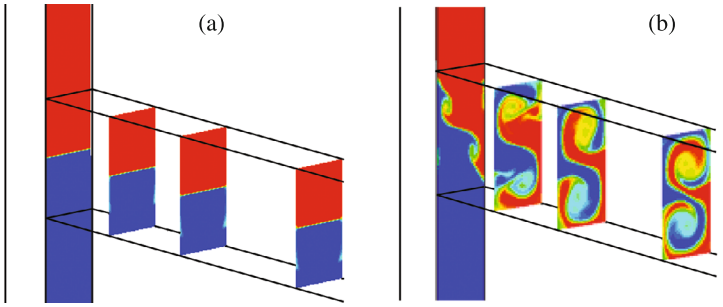

Fig. 3. Dye concentration contours in the channel cross-sections; Re = 140 (a) and 150 (b).

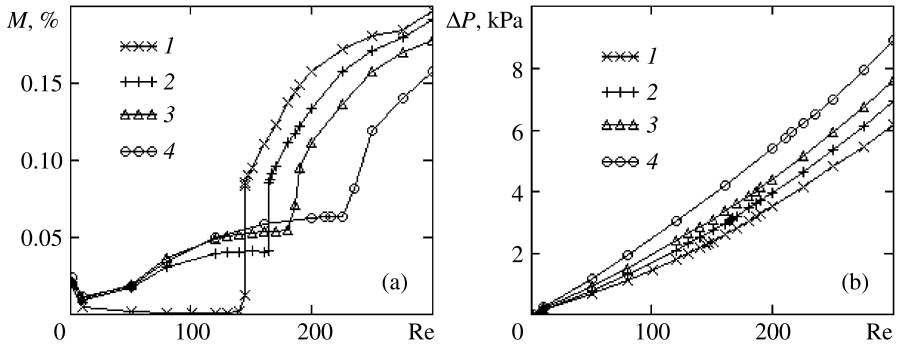

Fig. 4. Dependence of the mixing efficiency (a) and the pressure difference between the mixer entry and exit (b) on the Reynolds number; $\mu/\mu_0 = 1$ (*1*), 1.25 (*2*), 1.5 (*3*), and 2 (*4*).

Mixing of liquids with different viscosities. Below we consider the viscosity effect on the flow patterns in the microchannel. This calculation set differs from that described above in that viscosity of one of the liquids varied. As before, colored water was supplied through one channel entry. Through the other entry a liquid with the same density as the water but with different viscosity was supplied into the mixer. Three calculation sets with the liquids whose viscosities were greater than that of the water by factors of 1.25, 1.5, and 2 were performed. The Reynolds number was based on the water viscosity at the room temperature: $\mu = 0.001$ Pa s.

With increase in viscosity of one of the mixing liquids the flow considerably alters. At very small Reynolds numbers (less than 10) the structure of the flow and the mixing of the liquids with different viscosities is generally similar with that for two identical liquids. Because of this, in this case the mixing efficiency only slightly depends on the liquid viscosities (Fig. 4a). With increase in the Reynolds number vortices are generated in the channel and the difference in viscosities begins to manifest itself. In Fig. 5 we have plotted the dye concentration contours at Re = 120 and different viscosity ratios. Clearly that, as distinct from the case of the same viscosities of the mixing liquids, the surface of the contact between the media is no longer plane. The more viscous liquid forces the less viscous one out from the channel walls and, as it were, wraps around it. This is clearly visible in Fig. 5b and 5c. With increase in the viscosity ratio this effect builds up and the contact area of the mixing liquids grows. This leads to an increase in the mixing efficiency with increase in the viscosity ratio in this regime (Fig. 4).

An interesting behavior of the horseshoe-shaped Dean vortices shown in Fig. 5 can also be observable. Clearly, with increase in the viscosity ratio these vortices are generally conserved but the asymmetry about the central axis of the channel arises. As can be seen in Fig. 7, in the liquid with the greater viscosity the horseshoe-shaped vortex in the mixing channel decays more rapidly than in the liquid with the smaller viscosity. The greater the viscosity ratio the more clearly expressed this process. The similar asymmetry is observed in the secondary vortex formation region, at the junction between the entry channels and the mixing channel. In this case, it can be seen that the horseshoe-shaped Dean vortex situated in the water does not almost change with increase in the other liquid viscosity.

As in the flow of liquids with the same viscosities, with further increase in the Reynolds number the flow

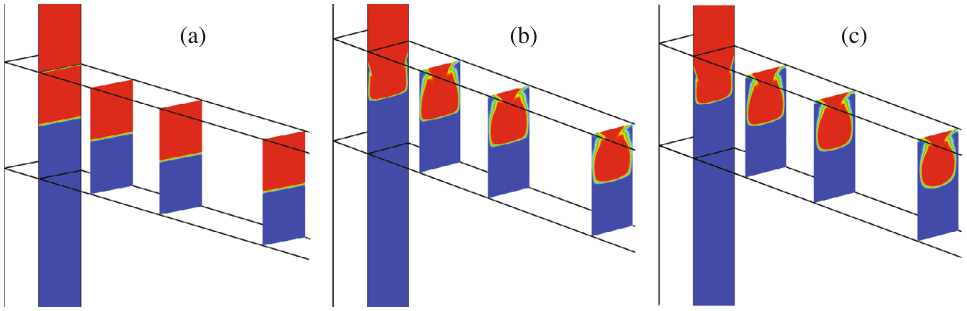

Fig. 5. Dye concentration contours; Re = 120 and $\mu/\mu_0 = 1$ (a), 1.5 (b), and 2 (c).

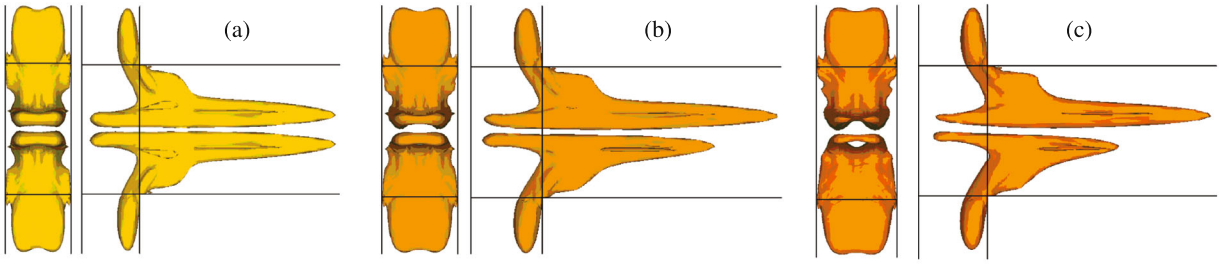

Fig. 6. λ_2 isosurfaces at the viscosity ratios $\mu/\mu_0 = 1$ (a), 1.5 (b), and 2 (c); the left sides of the figures represent the view from the dead wall of the mixer and the right sides are the side views; Re = 120.

turns up. However, as distinct from the case of equal viscosities, where transition occurs for the Reynolds numbers on the interval from 144 to 144.5, the transitional Reynolds number considerably changes. Thus, in the case in which the viscosity ratio is 1.25, the transition occurs on the Reynolds number interval from 164 to 165. For the viscosity ratio of 1.5 the flow turns up for Re = 181–183, and for the viscosity ratio of 2 at Re = 222–227. This is very clearly visible in Fig. 4a in which the mixing efficiency is plotted against the Reynolds number. The turnover and the symmetric-to-nonsymmetric flow pattern transition are accompanied by a sharp increase in the mixing efficiency. It can be seen from the plot that the Reynolds number associated with transition is displaced to the right with increase in the viscosity ratio. Moreover, it is visible that in the transition region the mixing efficiency jump becomes less clearly expressed.

The mixing pattern in the mixer after the flow turnover is shown in Fig. 7, Clearly that at different viscosity ratios the mixing structures are qualitatively very similar. Moreover, a layered S-shaped structure consisting of the mixing liquids is also formed. In this layered structure the contact surface of the mixing liquids is very developed which leads to a sharp increase in the mixing efficiency after the turnover. However, certain differences are also visible. The main difference is that in the more viscous liquid the vortex formed in the mixing channel after the turnover decays considerably more rapidly than the analogous vortex in the water. This is clearly visible from the isosurfaces presented in Fig. 8. The vortex situated in the lower part of the mixing channel occupied by the more viscous liquid is considerably shorter than the vortex in the water. With increase in the viscosity ratio this difference increases. The decay of one of the vortices in the mixing channel leads to the situation in which the contact surface of the mixing liquids is not so developed as in the water. This can be seen from the comparison with Fig. 7. For this reason, in the regime of the flow after the turnover the mixing efficiency decreases with increase in the viscosity ratio of the mixing media (Fig. 4a).

The pressure difference between the mixing channel entry and exit was also analyzed. Figure 4b presents the pressure difference between the entry in the channel with the more viscous liquid and the exit from the T-shaped microchannel. Clearly that, as in the case in which $\mu/\mu_0 = 1$, the pressure difference has no any special features in the region of transition from the symmetric to nonsymmetric flow regime of the more viscous liquid. Naturally that with increase in the viscosity ratio the pressure difference builds up.

Clearly that the results presented above show that viscosity has a considerable effect on the flow and the mixing in the microchannel under consideration. To generalize the results obtained we will base the Reynolds number on an effective mixture viscosity μ_m; then the Reynolds number can be determined as

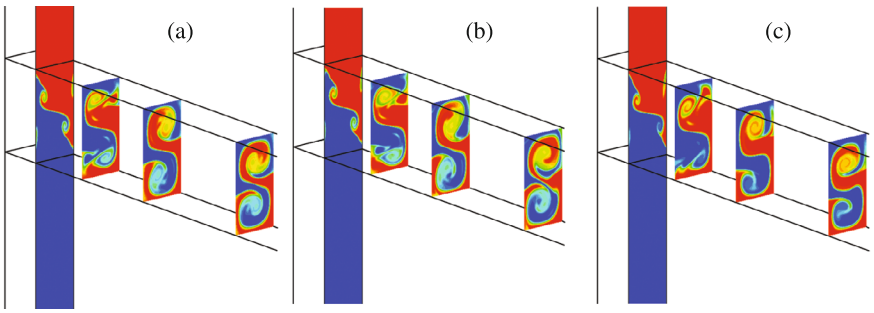

Fig. 7. Dye concentration contours; Re = 250 and $\mu/\mu_0 = 1$ (a), 1.5 (b), and 2 (c).

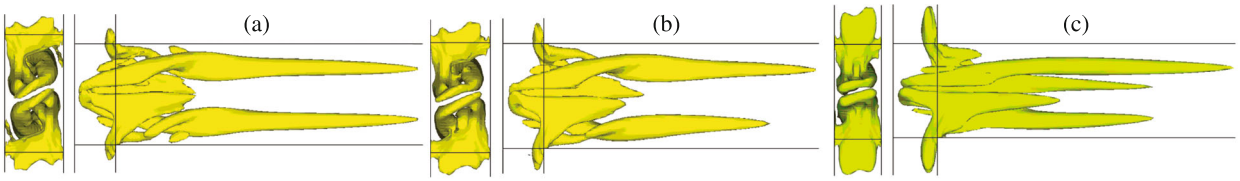

Fig. 8. λ_2 isosurfaces at the viscosity ratios $\mu/\mu_0 = 1$ (a), 1.5 (b), and 2 (c); the left sides of the figures represent the view from the dead wall of the mixer and the right sides are the side views; Re = 250.

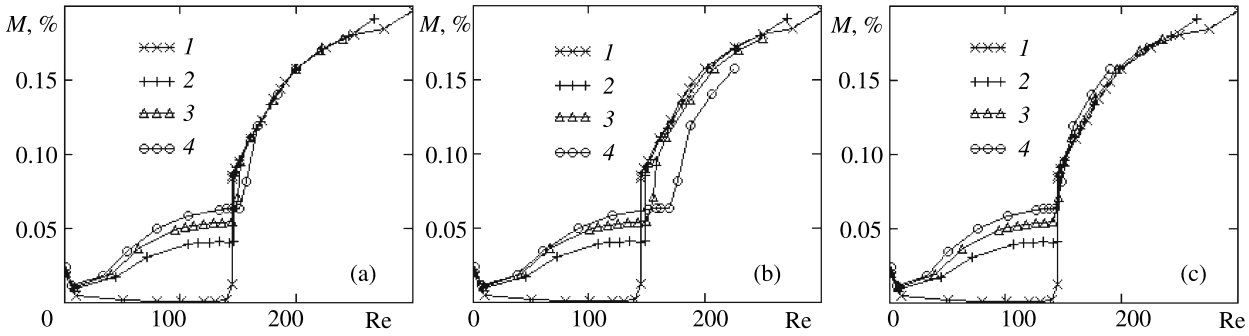

Fig. 9. Dependence of the mixing efficiency on the Reynolds number; $\mu_m = \mu_{m1}$ (a), μ_{m2} (b), and μ_{m3} (c); $\mu/\mu_0 = 1$ (*1*), 1.25 (*2*), 1.5 (*3*), and 2 (*4*).

$\mathrm{Re} = \rho U d_h/\mu_m$. In Fig. 9 we have plotted the mixing efficiency against the Reynolds number which was determined using three ways of preassigning the effective viscosity

$$\mu_{m1} = \frac{\mu_1 + \mu_0}{2}, \qquad \mu_{m2} = \frac{2\mu_0\mu_1}{\mu_1 + \mu_0}, \qquad \mu_{m3} = \sqrt{(\mu_1^2 + \mu_0^2)/2},$$

where μ_0 is the water viscosity, μ_1 is the other liquid viscosity, and μ_{m1}, μ_{m2}, and μ_{m3} are the arithmetic mean, the harmonic mean, and the square mean viscosities.

As can be seen from the data presented, the way of determining the mean viscosity has a considerable influence on the results. When the averaging is performed using the arithmetic and square means, transition occurs for the reduced Reynolds number of about 145 for all the viscosity ratios. After transition the data lie well on the same curve. The results obtained using the harmonic way of averaging are much worse. Thus, it is established that the transition point associated with the flow turnover can be described by the reduced Reynolds number $\mathrm{Re} = \rho U d_h/\mu_m$, where the effective viscosity μ_m is calculated using either the mean arithmetic μ_{m1} or the mean square μ_{m2} value.

Summary. The results of the modeling allow us to distinguish the following incompressible liquid flows in the T-type micromixer: a steady rotationless flow, jumpwise transition from the symmetric to the asymmetric flow pattern (turnover), and a steady nonsymmetric vortex flow. It is shown that a variation in the viscosity of one of the mixing liquids leads to a shift of the flow patterns but generally the flow regimes described above are conserved. It is established that on the symmetric flow range the mixing efficiency in-

creases with increase in the viscosity ratio which is due to an enlargement of the area of the contact between the mixing media, when the more viscous liquid flows around the less viscous one. In the nonsymmetric regime the mixing efficiency diminishes with increase in the viscosity ratio owing to the more rapid decay of the S-shaped vortex structure in the more viscous liquid and a decrease in the area of the contact between the mixing media. It is established that the flow of two liquids with different viscosities can be regarded as a self-similar flow with respect to the reduced Reynolds number.

The study was carried out with the partial support of the Russian Foundation for Basic Research (project No. 14-19-00312).

REFERENCES

1. P. Tabeling, *Introduction to Microfluidics*, Oxford Univ. Press, Oxford (2005).
2. G.E. Karnidakis, A. Beskok, and N. Aluru, *Microflows and Nanoflows. Fundamentals and Simulation*, Springer (2005).
3. R. Karnik, "Microfluidic Mixing," in: D. Li (ed.), *Encyclopedia of Microfluidics and Nanofluidics*, Springer (2008), p. 1177.
4. V. Rudyak and A. Minakov, "Modeling and Optimization of Y-Type Micromixers," Micromachines **5**, 886 (2014).
5. J. Aubina, D.F. Fletcherb, and C. Xuereb, "Design of Micromixers Using CFD Modeling," Chem. Eng. Sci. **60**, 2503 (2005).
6. D. Bokenkamp, A. Desai, X. Yang, Y.C. Tai, E.M. Marzluff, and S.L. Mayo, "Microfabricated Silicon Mixers for Submillisecond Quench-Flow Analysis," Anal. Chem. **70**, 232 (1998).
7. D.P. Gobby and A. Angeli, "Mixing Characteristics of T-Type Microfluidic Mixers," J. Micromech. Microeng. No. 11, 126 (2001).
8. M. Hoffmann, M. Schluter, and N. Rubiger, "Experimental Investigation of Liquid-Liquid Mixing in T-Shaped Micro-Mixers Using μ-LIF and μ-PIV," Chem. Eng. Sci. **61**, 2968 (2006).
9. D. Bothe, C. Stemich, and H.-J. Warnecke, "Theoretische und experimentelle Untersuchungen der Mischvorgänge in T-förmigen Mikroreaktoren. Teil 1. Numerische Simulation und Beurteilung des Strömungsmischens," CIT **76**, 1480 (2004).
10. D. Bothe, C. Stemich, and H.-J. Warnecke, "Fluid Mixing in a T-Shaped Micro-Mixer," Chem. Eng. Sci. **61**, 2950 (2006).
11. C. Stemich, "Theoretische und numerische Untersuchung des Stromungsmischens in einem T-förmigen Mikromischer," Padedrborn Univ., Dissertation (2006).
12. S. Dreher, N. Kockmann, and P. Woias, "Characterization of Laminar Transient Flow Regimes and Mixing in T-Shaped Micromixers," Heat Transfer Eng. **30**, 91 (2009).
13. A.V. Minakov, V.Ya. Rudyak, A.A. Gavrilov, and A.A. Dekterev, "Mixing in T-Type Micromixers at Moderate Reynolds Numbers," Teplofiz. Aeromekh. **19**, 577 (2012).
14. A. Minakov, V. Rudyak, A. Dekterev, and A. Gavrilov, "Investigation of Slip Boundary Conditions in the T-Shaped Microchannel," Int. J. Heat Fluid Flow **43**, 161 (2013).
15. A. Minakov, A. Yagodnitsina, A. Lobasov, V. Rudyak, and A. Bilsky, "Study of Fluid Flow in Micromixer with Symmetrical and Asymmetrical Inlet Conditions," La Houille Blanche No. 5, 12 (2013).
16. V. Ya. Rudyak, A.V. Minakov, A.A. Gavrilov, and A.A. Dekterev, "Modeling Flows in Micromixers," Teplofiz. Aeromekh. **17**, 601 (2010).
17. A.A. Gavrilov, A.V. Minakov, A.A. Dekterev, and V.Ya. Rudyak, "A Numerical Algorithm for Modeling Laminar Flows in an Annular Channel with Eccentricity," J. Appl. Industr. Math. **5**, 559 (2011).
18. S.V. Patankar, *Numerical Heat Transfer and Fluid Flow*, McGraw Hill, New York (1980).
19. Yu.A. Bystrov, S.A. Isaev, N.A. Kudryavtsev, and A.I. Leont'ev, *Numerical Modeling of the Vortex Intensification of Heat Transfer in Tube Arrays* [in Russian], Sudostroenie, St. Petersburg (2005).
20. J.H. Ferziger and M. Peric, *Computational Methods for Fluid Dynamics*, Springer, Berlin (2002).
21. B.P. Leonard, "A Stable and Accurate Convective Modeling Procedure Based on Quadratic Upstream Interpolation," Comp. Math. Appl. Mech. Eng. **19**, 59 (1979).
22. C.M. Rhie and W.L. Chou, "Numerical Study of the Turbulent Flow past an Airfoil with Trailing Edge Separation," AIAA J. **21**, 1525 (1983).
23. U. Trottenberg, W. Cornelis, C.W. Oosterlee, and A. Schúller, *Multigrid*, Acad. Press, New York (2001).